Chemical Engineering Journal 362 (2019) 81–88

Contents lists available at ScienceDirect

Chemical Engineering Journal

journal homepage: www.elsevier.com/locate/cej

Bioaccumulation and transformation of U(VI) by sporangiospores of *Mucor circinelloides*

Wencheng Song[a,b], Xiangxue Wang[a], Yubing Sun[a,c,*], Tasawar Hayat[c], Xiangke Wang[a,c,d,*]

[a] MOE Key Laboratory of Resources and Environmental System Optimization, College of Environmental Science and Engineering, North China Electric Power University, Beijing 102206, PR China
[b] Anhui Province Key Laboratory of Medical Physics and Technology, Center of Medical Physics and Technology, Hefei Institutes of Physical Science, Chinese Academy of Sciences, Hefei 230031, PR China
[c] Collaborative Innovation Center of Radiation Medicine of Jiangsu Higher Education Institutions and School for Radiological and Interdisciplinary Sciences, Soochow University, 215123 Suzhou, PR China
[d] NAAM Research Group, Faculty of Science, King Abdulaziz University, Jeddah 21589, Saudi Arabia

HIGHLIGHTS

- The number and morphology of sporangiospores changes obviously under U(VI) stress.
- Sporangiospores show efficient bioaccumulation of U(VI) from wastewater.
- The intracellular U(VI) of sporangiospores is reduced to U(IV).
- The reduced U(IV) is associated with a light element oxyanion ligand.

GRAPHICAL ABSTRACT

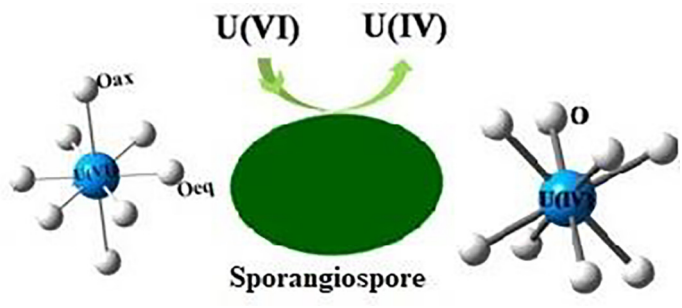

ARTICLE INFO

Keywords:
Sporangiospores
Bioaccumulation
U(VI)
XAFS

ABSTRACT

The bioaccumulation and transformation of U(VI) by sporangiospores of *Mucor circinelloides* under different environmental conditions (e.g., reaction time, pH, carbonate, sporangiospores concentration, and temperature) was investigated by batch, XPS and EXAFS techniques. The bioaccumulation kinetics and isotherms can be fitted by the pseudo-second-order kinetic mode and Langmuir model, respectively, due to the high correlation coefficient. The maximum bioaccumulation capacity of sporangiospores for U(VI) was 166.13 mg/g at pH 6.0, which was significantly higher than that of other mycelia or spores. The intracellular and extracellular morphology of sporangiospores were significantly changed after U(VI) bioaccumulation, and levels of intracellular H_2O_2, O_3^-, GPx and SOD compounds in sporangiospores increased significantly. XANES analysis confirmed that the intracellular U(VI) was reduced to U(IV) by sporangiospores, and U(IV) might be stably associated with oxygen-bearing functional groups by EXAFS analysis. These results show that the sporangiospores can be used a promising adsorbent for the bioaccumulation and transformation of U(VI) from aqueous solutions, which has important scientific significance for the immobilization of U(VI) in environmental remediation.

* Corresponding authors at: MOE Key Laboratory of Resources and Environmental System Optimization, College of Environmental Science and Engineering, North China Electric Power University, Beijing 102206, PR China.
E-mail addresses: sunyb@ncepu.edu.cn (Y. Sun), xkwang@ncepu.edu.cn (X. Wang).

https://doi.org/10.1016/j.cej.2019.01.020
Received 8 October 2018; Received in revised form 1 December 2018; Accepted 4 January 2019
Available online 05 January 2019
1385-8947/

1. Introduction

Due to the depletion and non-sustainability of fossil fuels, more and more countries pay attention to the development and utilization of economic and efficient nuclear energy, and consider or start the construction of nuclear power plants [1]. Uranium (^{235}U) is the main fuel for nuclear power in the world for a long time in the future. From its exploitation to the disposal of nuclear waste, radionuclides will enter the environment, which may endanger human health [2,3]. How to repair and control the pollutions of these radionuclides has attracted the attention of people all over the world. In most cases, physicochemical methods (e.g., flocculation, ultrafiltration, dialysis, and adsorption) are used to treat radionuclides in wastewater [4–8]. However, these methods are expensive to handle and are not easy to manage and operate, which cause secondary pollution.

In recent years, removal of radionuclides on microorganisms has become a research hotspot in the field of radionuclide remediation because of no secondary pollution, good effect and low cost [9–11]. Among them, the filamentous fungus is prone to grow in moist environments, especially in acidic media, which are similar to radionuclides-contaminated medium. The mycelium of filamentous fungal has been extensively applied to remove radionuclides due to high adsorption capacity and abundant surface groups. For example, Lujanienė et al. showed that approximately 100% of Pu(V) was removed by the filamentous fungus (i.e., *Penicillium chrysogenum*) at pH 4.1 [12]. Vinichuk et al. found that *Arbuscular mycorrhizal* (*Glomus mosseae*) presented the high adsorption capacity for ^{137}Cs in sandy loam soil and loam soil, and promoted sunflower [13]. However, Zhao et al. showed that the adsorption of U(VI) on *Pleurotus ostreatus* only reached ~20 mg/g at pH 4.0 [14]. The *Aspergillus niger* as a common resistant filamentous fungus was found to efficiently adsorb Co(II) and Eu(III) in our previous studies [15]. Besides, radionuclides could produce amounts of reactive oxygen species (H_2O_2 and O_3^-) in filamentous fungi under radionuclides stress, while antioxidant enzymes such as glutathione peroxidases (GPx) and total superoxide dismutases (SOD) were induced by filamentous fungi to deal with H_2O_2 and O_3^- damage [16–18].

X-ray absorption fine structure (XAFS) as a widespread synchrotron radiation technique has been applied to study the transformation mechanism of radionuclides on filamentous fungi [19]. Günther et al. found the formation of inner-sphere surface complexation between U (VI) and filamentous fungus by phosphate groups of cell by EXAFS analysis [20]. Yu et al. demonstrated that the filamentous fungus of *Acremonium strictum* promoted the conversion of lanthanides in the process of bivalent manganese biooxidation using XANES [21]. In our previous studies, it is observed that U(VI) can be reduced to U(IV) by *Mucor circinelloides*, while the reducing ability was significantly decreased in the presence of As(V) [22]. The effect of mycelia on radionuclides has been investigated, whereas little attention to the influence of spores on radionuclides was paid in these studies. In fact, the mycelium of filamentous fungi is inevitably mixed with spores. Filamentous fungi mainly rely on the production of a variety of asexual or sexual spores for reproduction, which has a strong reproductive ability in nature. Spores (containing conidiospores, sporangiospores, arthrospores, etc.) have different characteristics such as morphological color, long dormancy, and strong resistance [23–25]. However, few studies regarding bioaccumulation mechanism of U(VI) on spores of filamentous fungi using XAFS analysis were available.

Spores produced by *Mucor circinelloides* mainly were sporangiospores, and the production and morphology of sporangiospores were investigated in this study. The aims of this study were to (1) explore the bioaccumulation of radionuclide U(VI) by sporangiospores; (2) investigate oxidative stress and anti-oxidative stress levels of sporangiospores towards U(VI), (3) elucidate intracellular transformation mechanism of U(VI) in sporangiospores by XAFS technique. The results will provide the theoretical basis for the repair of radionuclide contamination by sporangiospores.

2. Experimental details

2.1. Materials and methods

The strain of *Mucor circinelloides* was screened, identified and preserved [22]. Briefly, the *Mucor circinelloides* culture after activation was transferred to Czapek-Dox liquid medium, and then incubated at 26 °C for 6 d to produce sporangiospores. These sporangiospores were harvested with Milli-Q water by a shaker with 100 rpm for 10 min prior to the subsequent experiments. The concentration of the sporangiospores in the suspension was calculated around 10^7 CFU/mL.

U(VI) stock solution (1000 mg/L) was prepared by dissolving $UO_2(NO_3)_2{\cdot}6H_2O$ (99.99% purity, Sigma-Aldrich) into Milli-Q water under glovebox conditions, and it was diluted for batch experiments from 5 mg/L to 300 mg/L. We synthesized UO_2(s) solid using the method of Ulrich et al [26]. All other reagents were purchased from Sinopharm Chemical Reagent Co. Ltd. (Shanghai, China) and used directly without further purification.

2.2. Characterization of sporangiospores

The morphologies of sporangiospores were performed using SEM (FEI-JSM 6320F, Japan) with an energy dispersive X-ray analysis (EDX) and TEM (JEM-2010, Japan). Zeta potentials were measured using 90 Plus particle size analyzer with BI-Zeta option (Brookhaven Instruments Corporation, TX, USA). Briefly, fungal sporangiospores before and after U(VI) bioaccumulation were added in 5% glutaraldehyde at 4 °C for 4 h, and then were washed with 0.1 mol/L phosphate buffer. The suspensions were dehydrated by sequentially adding 10, 30, 70, 90 and 100% ethanol, finally critical-point-dried under room temperature. A drop suspension was on copper grids with gold coated for SEM analysis. However, the samples for TEM analysis were pre-fixed with 5% glutaraldehyde and were infiltrated with resin, and then were sectioned to a 70-nm thickness with an ultramicrotome (Leica EM UC7, Austria).

2.3. Preparation and analysis of XANES and EXAFS spectra

The samples for XANES and EXAFS spectra were prepared as followed protocols: the Czapek-Dox liquid medium containing different U (VI) concentrations and mycelia were added into 250 mL flask bottles. The values of pH were adjusted to pH 6.0 at 26 °C. The suspensions were reacted at glovebox conditions for 5 h, 5 d and 15 d. After reaction, the solid were separated from liquid phase by centrifuging at 6000 rpm for 30 min and washing with sterile deionized water. The wet pastes of sporangiospores were sealed in Teflon sample holders with Kapton tape for XANES and EXAFS analysis. U L_{III}-edge XANES and EXAFS spectra were collected using Si (111) monochromator with 32-element Ge detector at Shanghai Synchrotron Radiation Facility (BL14W, Shanghai, China). The analysis and fitting of EXAFS data were analyzed using Athena and Artemis of IFFEFIT 7.0 software, respectively [27]. The theoretical paths of U-Oax, U-Oeq, U-C shells were derived from uranyl acetate.

2.4. Batch bioaccumulation experiments

Batch bioaccumulation experiments of U(VI) sporangiospores on under various environmental conditions (e.g., reaction time, pH, carbonate, sporangiospores concentration, and temperature) were carried out in 10-mL plastic centrifuge tube under glovebox conditions. The bioaccumulation kinetics was conducted by adding 1.5 mg sporangiospores and 30 mg/L of U(VI) into 10-mL plastic centrifuge tube at pH 6.0. The effect of pH on U(VI) bioaccumulation at 0, 20 and 100 mg/L Na_2CO_3 was carried out over wide pH ranging from 2.0 to 11.0 by adding ignore volume of 1.0–0.01 mol/L HCl or NaOH. Effect of

sporangiospores doges and U(VI) concentration under different temperature (299, 319 and 339 K) on U(VI) bioaccumulation was performed at pH = 6.0 for exposure time 48. Then the solid was separated from liquid phase by centrifugation at 8000 rpm for 15 min. After bioaccumulation equilibrium, the solid was separated from the liquid phase by centrifugation at 8000 rpm for 15 min. The concentration of U (VI) in supernate was measured by Inductively Coupled Plasma-mass Spectrometry (ICP-MS, Shimazu). The blank experiments without sporangiospores indicated that U(VI) accumulation to tube walls was negligible. Bioaccumulation percentage (%) and capacity (Q_e, mg/g) were described as Eqs. (1) and (2):

$$\text{Bioaccumulation } \% = (C_0 - C_e) \times 100\%/C_0 \quad (1)$$

$$Q_e = (C_0 - C_e) \times V/m \quad (2)$$

where C_0 and C_e (mg/L) are initial and equilibrium concentrations of U (VI), respectively. m and V are the mass of adsorbent and volume of suspension, respectively. All experimental data were the average of triplicate determinations and error bars of plotted data were given within ± 5%.

2.5. Analysis of biochemical parameters

The change in H_2O_2, O_3^-, GPx and SOD levels of sporangiospores after 0, 100, 200 and 300 mg/L U(VI) exposure as a function of exposure time were performed at T = 299 K and pH = 6.0. Briefly, 1.5 mg sporangiospores and U(VI) solution with different concentrations (0, 100, 200 and 300 mg/L) were added into 10 mL centrifuging tubes, then pH was adjusted to 6.0 under glovebox conditions and were reacted at different reaction times. After centrifugation, sporangiospores were frozen under liquid nitrogen and then were ground into powder, and then 10 mL of extraction solution (50 mmol/L Na_3PO_4, 1% PVP, and 0.1 mmol/L EDTA) was added. The concentrations of H_2O_2 and O_3^- in sporangiospores after U(VI) exposure were detected using a Hydrogen Peroxide Test kit and Ozone test kit, respectively. The GPx activity was assayed by using the Ransel kit (Randox Laboratories Ltd., UK) [28], and SOD activity was monitored by measuring its ability to inhibit photochemical reduction of nitro blue tetrazolium at 560 nm [29].

2.6. Statistical analysis

The data obtained from triple experiments were presented as means ± S.D by SPSS 19.0. The fulfilment of the one-way analysis of variance (ANOVA) requirements, specifically the normal distribution of the residuals and the homogeneity of variance, was tested by means of the Shapiro–Wilk's and the Levene's tests, respectively. Statistical significances between groups were evaluated by ANOVA with a Student-Newman-Keuls post-test (if data fulfilled homoscedasticity) or Tamhane's T2 post-test (if data did not fulfill homoscedasticity). A p-value < 0.05 between two independent groups was considered to the statistically significant difference.

3. Results and discussion

3.1. Production of sporangiospores

Fig. 1a shows the production of sporangiospores under different U (VI) stress. The production of sporangiospores in the absence of U(VI) increased logarithmically in the first 6 days (d), and then production rate increased slowly after 6 d. However, the number of sporangiospores significantly decreased with increasing U(VI) concentrations. After 8 d of exposure, approximately 50, 20 and 5 × 10^8 U/mg were observed at 0, 100 and 300 mg/L U(VI), respectively. The significant difference ($p < 0.05$) between the addition of 300 mg/L U(VI) and 100 mg/L U(VI) was observed, whereas no significant difference between the addition of 200 mg/L U(VI) and 100 mg/L U(VI) was found. This results indicated that the growth of mycelia and sporangiospores were suppressed under U(VI) stress [22].

3.2. Characterization of sporangiospores

Fig. 1b shows the zeta potentials of sporangiospores under different pH conditions. The zeta potential of sporangiospores is negative at pH > 3.0. Moreover, the values of zeta potential significantly decreased with the increase of pH. Due to the existence of a large number of polar surface groups on of sporangiospores, these surface groups were ionized, and the double electric layer was formed when sporangiospores was dissolved in the aqueous solutions [30–32]. This results of zeta potentials indicated that sporangiospores had negative charges on the surface, which are responsible for high effective adsorption of positive ions by electrostatic attraction at low pH.

The SEM images of sporangiospores before and after adding U(VI) were shown in Fig. 2a and b, respectively. Without U(VI), the abundant short rod-like sporangiospores were accumulated together (Fig. 2a). However, the morphology of most sporangiospores after adding U(VI) appeared sunken and damaged (Fig. 2b) [30]. The EDX spectra indicated that the main constituents of sporangiospores after adding U (VI) were C, O, U, N, P, K and S (the area indicated with golden arrow in Fig. 2b). TEM images of sporangiospores before and after adding U(VI) were shown in Fig. 2c and d, respectively. As shown in Fig. 2c, the particle sizes of sporangiospores were approximately 4 μm length × 2 μm width. After adding U(VI), it was observed that all visible cell wall displayed the blur and shrink significantly. The electron-dense areas (indication with golden arrow in Fig. 2d) were found around intracellular and extracellular sporangiospores after U(VI) exposure. The same phenomenon was found in *Aspergillus niger* under Cr (VI) stress [33]. Besides, U(VI) could lead to lysis of sporangiospores and release of intracellular substances, resulting in the death of sporangiospores [34].

3.3. Effect of reaction time

Fig. 3a shows the U(VI) bioaccumulation by sporangiospores under different reaction time. The high bioaccumulation rate (more than 80%) at the first stage (0–24 h), could be attributed to the quick combination of U(VI) with the abundant functional groups of the sporangiospores. At the second stage (24–48 h), the low bioaccumulation rate was due to intraparticle diffusion of U(VI) into the intracellular process [35]. The pseudo-first-order and pseudo-second-order kinetic models were employed to simulate accumulation kinetics (see Table S1 in SI for details). Compared to the pseudo-first-order kinetic model ($R^2 = 0.953$), the pseudo-second-order kinetic model can better fit the kinetics of U(VI) bioaccumulation by sporangiospores ($R^2 = 0.999$). Wang and Cui demonstrated that the adsorption kinetic of Cu^{2+} on *Aspergillus niger* was well fitted by pseudo-second-order kinetic model [30].

3.4. pH effect

Fig. 3b showed the effect of pH on U(VI) bioaccumulation by sporangiospores with different Na_2CO_3 concentrations. It was observed that the bioaccumulation amount rapidly increased from pH 2.0 to 5.0, and high bioaccumulation was maintained between pH 5.0 and 7.0, and the bioaccumulation amount rapidly decreased at pH > 7.0. The speciation of U(VI) in aqueous solution is calculated by MINEQL 3.0 code and their chemical equilibrium constants were derived from Lawrence Livemore National Laboratory (LLNL) data [36]. More details regarding the distribution of U(VI) speciation were showed in Fig. S1 and Table S2 in SI. The main U(VI) species in the absence of carbonate was mainly UO_2^{2+} and $UO_2(OH)_4^{2-}$ species at pH < 5.0 and pH > 8.0, respectively, whereas $UO_2(CO_3)_2^{2-}$ and $UO_2(CO_3)_3^{4-}$ species in the presence

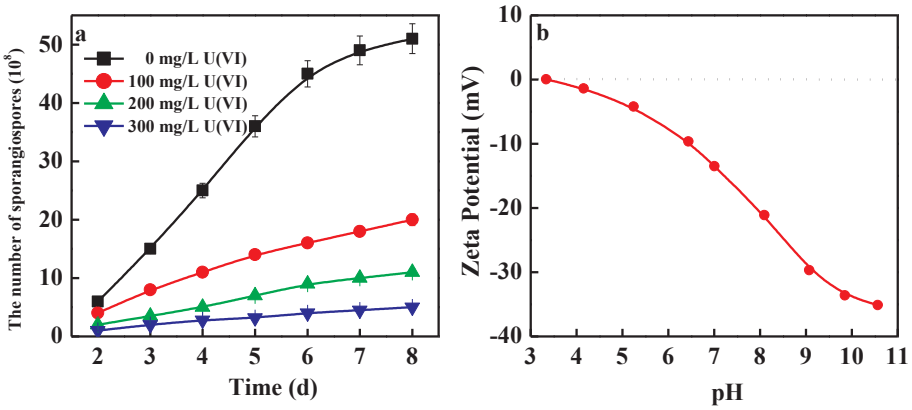

Fig. 1. a: The number of sporangiospores (10^8) grown under different U(VI) stress; b: Zeta potential.

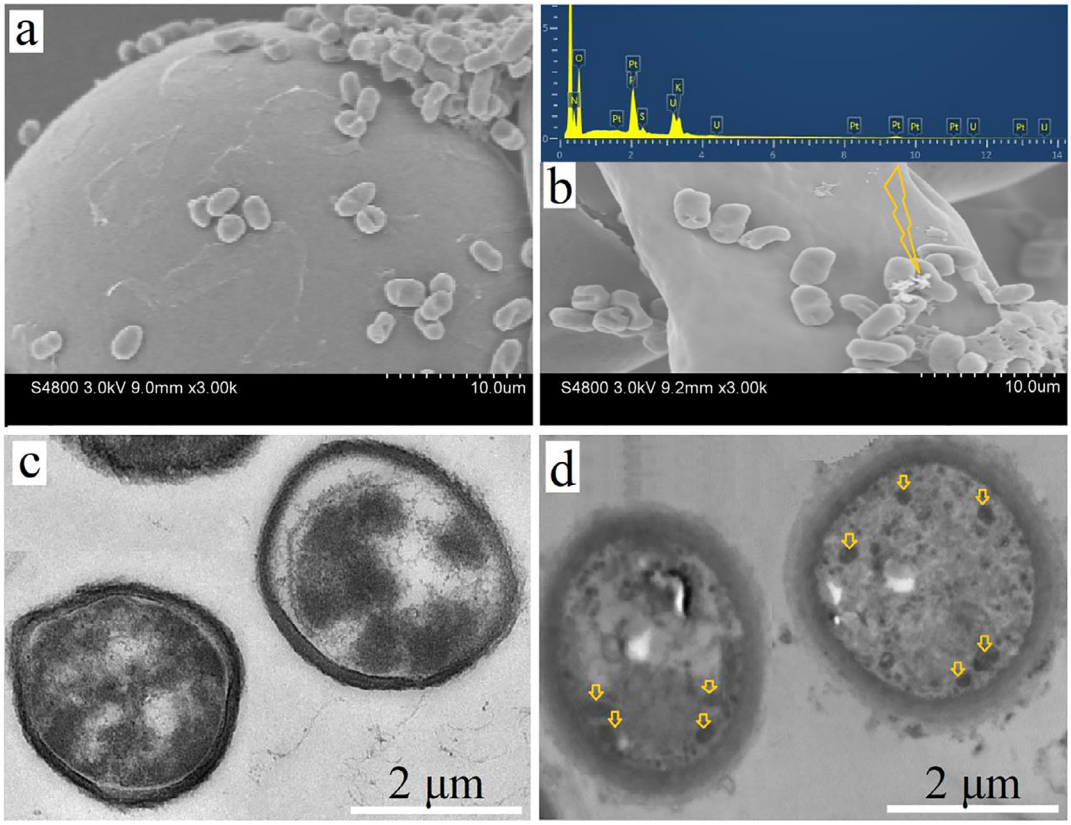

Fig. 2. Characterization of sporangiospores. a and b: SEM images of sporangiospores under 0 and 200 mg/L U(VI) stress, respectively; c and d: TEM images of sporangiospores under 0 and 200 mg/L U(VI) stress, respectively, T = 299 K.

of carbonate were observed at pH > 8.0. As shown in Fig. 1B, the negative charge of sporangiospores was observed at pH > 3.0. Therefore, the increased bioaccumulation of U(VI) by sporangiospores at pH 2.0–7.0 was attributed to the surface complexation and electrostatic attraction between positive U(VI) species and negatively charged sporangiospores. The decreased accumulation of U(VI) at pH > 7.0 could be due to the electrostatic repulsion between negative U(VI)-carbonate complexes and negatively charged sporangiospores.

3.5. Carbonate effect

Fig. 3b also showed the effect of carbonate on U(VI) bioaccumulation from pH 2.0 to pH 11.0. U(VI) bioaccumulation on sporangiospores at pH < 6.0 remarkably increase with the increase in Na_2CO_3, whereas the bioaccumulation rate of U(VI) on sporangiospores dramatically decreased with increasing Na_2CO_3 at pH > 7.0. The increased bioaccumulation of U(VI) with the increase of Na_2CO_3 at pH 0 ~ 5.0 could be due to the formation of complexes such as SO-UO_2-CO_3 due to the electrostatic attraction [3]. As shown in Fig. S1b, the main carbonato-complexes are observed at pH 6.0–10.0, such as $(UO_2)_2CO_3(OH)_3^-$, $UO_2(CO_3)_2^{2-}$ and $UO_2(CO_3)_3^{4-}$ species. The decreased accumulation of U(VI) at pH > 7.0 was due to the mutual exclusion of negatively charged U(VI) and negatively charged sporangiospores.

3.6. Effect of sporangiospores concentration

Fig. 3c showed the effect of sporangiospores concentration on U(VI) bioaccumulation on sporangiospores. The bioaccumulation percentage of U(VI) in solution increased with the increase of sporangiospores concentration and reached the maximum bioaccumulation at 0.3 g/L,

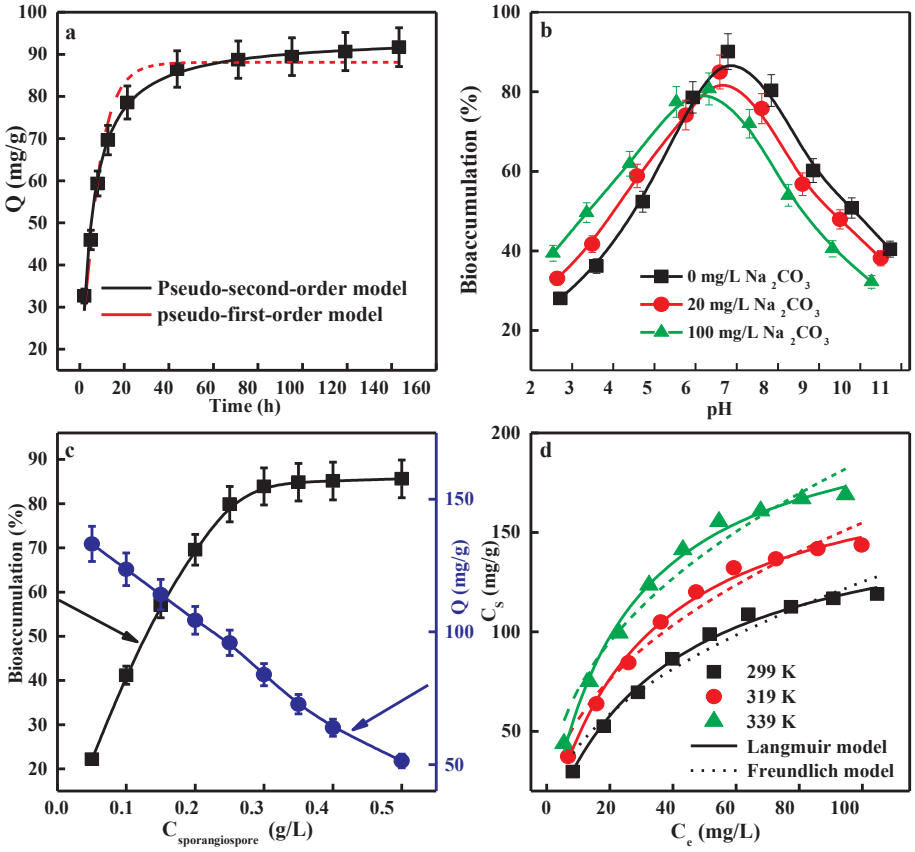

Fig. 3. a: Kinetics of U(VI) on sporangiospores, pH = 6.0, C_0 = 30 mg/L, m/v = 0.25 g/L, T = 299 K; b: Effect of pH on bioaccumulation, C_0 = 30 mg/L, m/v = 0.25 g/L, T = 299 K, exposure time = 48 h; c: Effect of sporangiospores concentration on the bioaccumulation, pH = 6.0, T = 299 K, exposure time = 48 h; d: bioaccumulation isotherms of U(VI) on sporangiospores, pH = 6.0, T = 299 K, exposure time = 48 h.

and then almost remained unchanged with increasing sporangiospores concentration. As sporangiospores concentration increased, the surface functional group of sporangiospores increased, providing more effective reactive sites for U(VI) bioaccumulation. It also can be seen from Fig. 3c that the maximum bioaccumulation capacity of U(VI) of sporangiospores tended to decrease with the increase of sporangiospores concentration. The bioaccumulation site of sporangiospores surface presents different binding energies. At lower sporangiospores concentration, the surface sites can complex U(VI) in solution, and the sites quickly reached bioaccumulation saturation, leading to the high bioaccumulation of U(VI). At higher sporangiospores concentration, the surface site with low binding energy was almost occupied, whereas U (VI) was not easily adsorbed on a surface site with high binding energy, causing a decrease in the amount of U(VI) bioaccumulation [37].

3.7. Bioaccumulation isotherms

Fig. 3d showed the bioaccumulation isotherms of U(VI) on sporangiospores at 299, 319 and 339 K. The previous studies demonstrated that bioaccumulation capacity was strongly dependent on temperature [38,39]. At low initial U(VI) concentrations, the U(VI) bioaccumulation increased with the increase of U(VI) concentration, and then the high-level bioaccumulation was observed at high initial U(VI) concentrations. The data of isothermal bioaccumulation of U(VI) on sporangiospore were simulated by Langmuir and Freundlich models. The relevant parameters of the Langmuir and Freundlich models were listed in Table S3 in SI. It can be seen from Fig. 3d that the Langmuir model was more suitable for the simulation of U(VI) bioaccumulation by sporangiospores. At pH 6.0, T 299 K, the maximum bioaccumulation capacities (C_{smax}) of U(VI) bioaccumulation by sporangiospores was 166.13 mg/g, which was significantly higher than that of other mycelia or spores (Table S4 in SI).

3.8. Detection of intracellular H_2O_2 and O_3^- levels

The survivability of sporangiospores under U(VI) stress was conducive to the U(VI) bioaccumulation. Toxicological parameters (H_2O_2, O_3^-, GPX and SOD levels) were conducted to detect the resistance of sporangiospores against U(VI) poisoning. To test the possibility of U(VI) induced oxidative stress, intracellular H_2O_2 and O_3^- levels was investigated in Fig. 4. The concentration of H_2O_2 and O_3^- in sporangiospores after adding U(VI) significantly increased with the increase of culture time. At 1 d of culture time, approximately 55 and 35 mg/L of H_2O_2 were detected at 300 and 100 mg/L U(VI), respectively. Similarly, 1.0 and 0.7 mg/L of O_3^- were observed at 300 and 100 mg/L U(VI), respectively. The significant differences ($p < 0.05$) were observed at 300 mg/L U(VI) and 200 mg/L U(VI). Similar phenomena were reported that A431 cells responded induced by silver nanoparticles [40].

3.9. Antioxidase activity

The cells generally produce many antioxidant enzymes (e.g., GPx and SOD) and antioxidants to resist oxidative stress, which can maintain cell homeostasis [18,41–43]. Fig. 5 showed the GPx and SOD activity of sporangiospores exposure with different U(VI) concentrations. The GPx activity increased slowly as culture time increased before 6 d, and then it remained almost unchanged after 6 d (Fig. 5a). The similar trends were also observed for the SOD activity (Fig. 5b). At 6 d of culture time, approximately 80 and 30 U/mg of GPx content were observed in the absence and presence (300 mg/L) of U(VI), respectively. The significant differences were observed between 100, 200, and 300 mg/L U(VI) ($p < 0.05$). Yin et al. found that SOD as superoxide played a critical role in the reduction of silver [44]. Azevedo Neto et al. also demonstrated that GPx and SOD activities in leaves of maize under salt stress increased with increasing culture time [45].

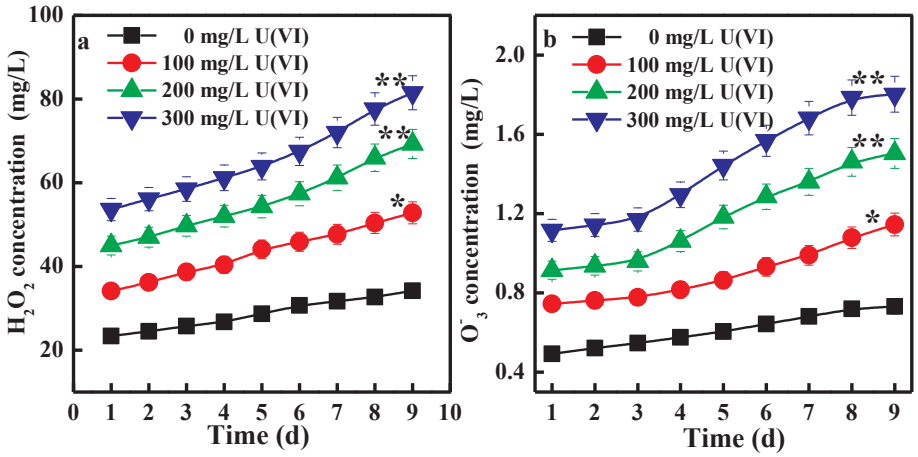

Fig. 4. Concentration of H_2O_2 and O_3^- in sporangiospores. H_2O_2 (a) and O_3^- (b) concentration was detected at different day.

3.10. XANES and EXAFS analysis

Fig. 6a and 6b show the uranium L_{III}-edge XANES and EXAFS analysis at different conditions, respectively. Aqueous UO_2^{2+} and solid UO_2 were used as standards for test samples. As shown in Fig. 6a, the valence state of intracellular U changed significantly with reaction time. The absorption edge energies of XANES spectra at 17,175 and 17178 eV correspond to UO_2(s) and UO_2^{2+}, respectively [46–48]. The absorption-edge energies of U-bearing sporangiospores at 5 h and 15 d were similar to that of UO_2^{2+} and UO_2(s), respectively, whereas the peak position of U-bearing sporangiospore at pH 6 and 5 d was located between UO_2(s) and UO_2^{2+}. The previous studies demonstrated that filamentous fungi as a natural antioxidant displayed the strong reduction capacity [22,49]. The results of XANES indicated that the main species of uranium bioaccumulation sporangiospores after exposure 5 h and 15 d were U(VI) and U(VI), respectively, whereas partial U(VI) was reduced to U(IV) for sporangiospores after exposure 5 d.

EXAFS technology was also used to determine the coordination microenvironment of uranyl ions with proteins [50,51]. As shown in Fig. 6b, the first and second Fourier transform (FT) feature for U-bearing sporangiospores at pH 6 and 5 h and 5 d can be fitted by a two axial oxygen shell ($U–O_{ax}$) at 1.8 Å and five equational oxygen shell ($U-O_{eq}$) at 2.32 Å, respectively [52]. The weak peaks at 2.7 Å can be fitted by the U-C shell, indicating the formation of inner-sphere surface complexation (Table 1) [52]. The standard EXAFS spectra of a crystalline UO_2 were derived from the previous study [53]. Enough interested, the new FT feature for U-bearing sporangiospores at 5 d and 15 d at approximately 3.89 Å can be fitted by U-U coordination in UO_2, moreover U-U coordination number and coordination peak significantly increased with increasing culture time, indicating that U(VI) was reduced to U(IV) [54]. However, the other U-S/N shell was not observed due to the coordination with hard oxygen atoms rather than soft sulfur atoms [55]. Keramidas et al. also demonstrated that UO_2^{2+} was more prone to coordination with carboxylic acid groups [56]. Therefore, the results of EXAFS analysis indicated the high effective bioaccumulation of U(VI) on sporangiospores by inner-sphere surface complexation. The absorbed U(VI) can gradually be reduced to U(IV) with increasing culture time [53].

4. Conclusions

We investigated the ability of immobilised sporangiospores of *Mucor circinelloides* to bind and remove U(VI). The bioaccumulation of radionuclides U(VI) by sporangiospores was mainly influenced by time, pH, carbonate, sporangiospores concentration, and temperature. The bioaccumulation equilibrium fitted with the Langmuir model, and the C_{smax} of sporangiospores was 166.13 mg/g at pH = 6.0, T = 299 K, which was significantly higher than that of other mycelia or spores. The intracellular and extracellular morphological structure changed significantly from SEM and TEM, and levels of intracellular H_2O_2, O_3^-, GPx and SOD compounds in sporangiospores increased significantly under U(VI) stress. XANES analysis confirmed that the intracellular U (VI) of sporangiospores was reduced to U(IV), and reduced U(IV) might be associated with a light element oxyanion ligand by using EXAFS analysis. The results demonstrate the feasibility and effectiveness for the removal of U(VI) from wastewater and suggest the potential for the use of this biomaterial for the removal of other radionuclides.

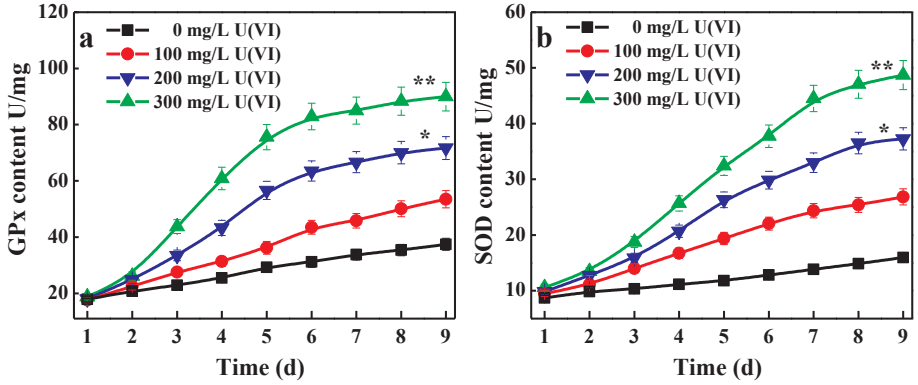

Fig. 5. Concentration of GPx and SOD in sporangiospores. GPx (a) and SOD (b) concentration was detected at different day.

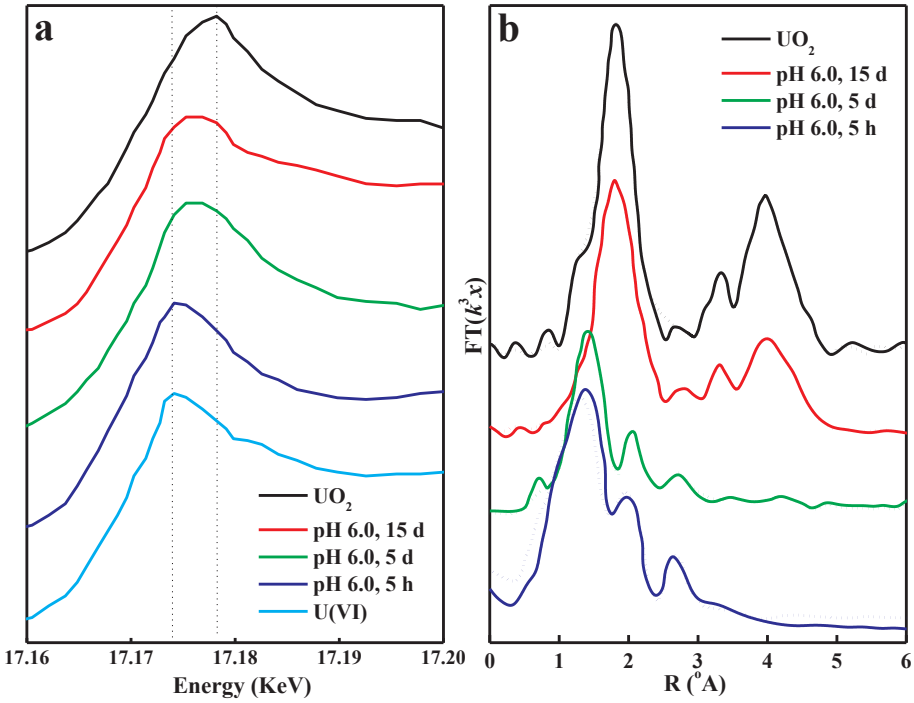

Fig. 6. Uranium L_{III}-edge XANES (a) and EXAFS (b) spectra of U(VI) bioaccumulation in sporangiospores at different time, Solid and dash lines represent experimental spectra and spectral fits, respectively.

Table 1
Uranium L_{III}-edge EXAFS spectra for U(VI) bioaccumulation by sporangiospores at different conditions.

Samples	Shell	R(Å)[a]	CN[b]	σ^2 (Å^2)[c]
pH = 6.0, t = 5 h	U–O_{ax}	1.79	2.01	0.008
	U-O_{eq}	2.35	5.51	0.006
	U-C	2.70	3.60	0.004
pH = 6.0, t = 5 d	U–O_{ax}	1.82	2.02	0.002
	U-O_{eq}	2.32	5.11	0.004
	U-C	2.69	2.70	0.004
	U–U	3.89	3.69	0.005
pH = 6.0, t = 15 d	U–O	2.33	4.04	0.025
	U-C	2.71	1.90	0.007
	U–U	3.92	5.61	0.006

[a] R is the bond distance.
[b] CN is coordination numbers of neighbors.
[c] σ^2 is the Debye-Waller.

Acknowledgements

This research was supported by National Natural Science Foundation of China (21876179, 21607156, 21822602), and the Priority Academic Program Development of Jiangsu Higher Education Institutions, the Collaborative Innovation Center of Radiation Medicine of Jiangsu Higher Education Institutions, and the Fundamental Research Funds for the Central Universities (JB2015001) are acknowledged.

Appendix A. Supplementary data

Supplementary data to this article can be found online at https://doi.org/10.1016/j.cej.2019.01.020.

References

[1] A. Richard, C. Rozsypal, J. Mercadier, D.A. Banks, M. Cuney, M.C. Boiron, M. Cathelineau, Giant uranium deposits formed from exceptionally uranium-rich acidic brines, Nat. Geosci. 5 (2012) 142–146.
[2] H. Geckeis, J. Luetzenkirchen, R. Polly, T. Rabung, M. Schmidt, Mineral-water interface reactions of actinides, Chem. Rev. 113 (2013) 1016–1062.
[3] Y.B. Sun, J.X. Li, X.K. Wang, The retention of uranium and europium onto sepiolite investigated by macroscopic, spectroscopic and modeling techniques, Geochim. Cosmochim. Acta 140 (2014) 621–643.
[4] D.P. Sheng, L. Zhu, C. Xu, C.L. Xiao, Y. Wang, Y.L. Wang, Y.X. Wang, L.H. Chen, J. Diwu, J. Chen, Z.F. Chai, T.E. Albrecht-Schmitt, S.A. Wang, Efficient and selective uptake of TcO_4^- by a cationic metal–organic framework material with open Ag^+ sites, Environ. Sci. Technol. 51 (2017) 3471–3479.
[5] L. Xu, T. Zheng, S.T. Yang, L.J. Zhang, J.Q. Wang, W. Liu, L.H. Chen, J. Diwu, Z.F. Chai, S.A. Wang, Uptake mechanisms of Eu(III) on hydroxyapatite: a potential permeable reactive barrier backfill material for trapping trivalent minor actinides, Environ. Sci. Technol. 50 (2016) 3852–3859.
[6] A. Veelen, J.R. Bargar, G.T.W. Law, G.E. Brown, R.A. Wogelius, Uranium immobilization and nanofilm formation on magnesium rich minerals, Environ. Sci. Technol. 50 (2016) 3435–3443.
[7] Y.B. Sun, S.H. Lu, X.X. Wang, C. Xu, J.X. Li, C.L. Chen, J. Chen, T. Hayat, A. Ahmed, N.S. Alharbi, X.K. Wang, Plasma-facilitated synthesis of amidoxime/carbon nanofiber hybrids for effective enrichment of ^{238}U(VI) and ^{241}Am(III), Environ. Sci. Technol. 51 (2017) 12274–12282.
[8] Z.Y. Zhuang, H. Chen, Z. Lin, Z. Dang, Mn_2O_3 hollow spheres synthesized based on an ion-exchange strategy from amorphous calcium carbonate for highly efficient trace-level uranyl extraction, Environ. Sci. Nano 3 (2016) 1254–1258.
[9] R. Tkavc, V.Y. Matrosova, O.E. Grichenko, C. Gostinčar, R.P. Volpe, P. Klimenkova, E.K. Gaidamakova, C.E. Zhou, B.J. Stewart, M.G. Lyman, S.A. Malfatti, B. Rubinfeld, M. Courtot, J. Singh, C.L. Dalgard, T. Hamilton, K.G. Frey, N. Gunde-Cimerman, L. Dugan, M.J. Daly1, Prospects for fungal bioremediation of acidic radioactive waste sites: characterization and genome sequence of *Rhodotorula taiwanensis* MD1149, Front. Microbial. 8 (2017) 1–21.
[10] C.C. Ding, W.C. Cheng, Y.B. Sun, X.K. Wang, Effects of *Bacillus subtilis* on the reduction of U (VI) by nano-Fe^0, Geochim. Cosmochim. Acta 165 (2015) 86–107.
[11] Y.B. Sun, R. Zhang, C.C. Ding, X.X. Wang, W.C. Cheng, C.L. Chen, X.K. Wang, Adsorption of U(VI) on sericite in the presence of *Bacillus subtilis*: a combined batch, EXAFS and modeling techniques, Geochim. Cosmochim. Acta 180 (2016) 51–65.
[12] G. Lujanienė, L. Levinskaitė, A. Kačergius, M. Gavutis, Sorption of plutonium to bacteria and fungi isolated from groundwater and clay samples, J. Radioanal. Nucl. Chem. 311 (2017) 1393–1399.
[13] M. Vinichuk, A. Mårtensson, T. Ericsson, K. Rosén, Effect of *arbuscular mycorrhizal* (AM) fungi on ^{137}Cs uptake by plants grown on different soils, J. Environ. Radioact. 115 (2013) 151–156.
[14] C. Zhao, J. Liu, H. Tu, F. Li, X. Li, J. Yang, J. Liao, Y. Yang, N. Liu, Q. Sun, Characteristics of uranium biosorption from aqueous solutions on fungus *pleurotus ostreatus*, Environ. Sci. Pollut. Res. 23 (2016) 24846–24856.
[15] W.C. Song, J. Liang, T. Wen, X.X. Wang, J. Hu, T. Hayat, A. Ahmed, X.K. Wang, Accumulation of Co(II) and Eu(III) by the mycelia of *Aspergillus niger* isolated from radionuclide-contaminated soils, Chem. Eng. J. 304 (2016) 186–193.
[16] S. Zhang, X. Zhang, C. Chang, Z. Yuan, T. Wang, Y. Zhao, Z. Zhang, Improvement of

tolerance to lead by filamentous fungus *Pleurotus ostreatus* HAU-2 and its oxidative responses, Chemosphere 150 (2016) 33–39.
[17] J. Schneider, J. Bundschuh, W. Melo Rangel, L.R.G. Guilherme, Potential of different AM fungi (native from As-contaminated and uncontaminated soils) for supporting *Leucaena leucocephala* growth in As-contaminated soil, Environ. Pollut. 224 (2017) 125–135.
[18] C. Li, L. Shi, D. Chen, A. Ren, T. Gao, M. Zhao, Functional analysis of the role of glutathione peroxidase (GPx) in the ROS signaling pathway, hyphal branching and the regulation of ganoderic acid biosynthesis in *Ganoderma lucidum*, Fungal Genet. Biol. 82 (2015) 168–180.
[19] X. Vázquez-Campos, A.S. Kinsela, R.N. Collins, B.A. Neilan, N. Aoyagi, T.D. Waite, Uranium binding mechanisms of the acid-tolerant fungus *Coniochaeta fodinicola*, Environ. Sci. Technol. 49 (2015) 8487–8496.
[20] A. Günther, J. Raff, M.L. Merroun, A. Roßberg, E. Kothe, G. Bernhard, Interaction of U (VI) with *Schizophyllum commune* studied by microscopic and spectroscopic methods, Biometals 27 (2014) 775–785.
[21] Q. Yu, T. Ohnuki, K. Tanaka, N. Kozai, S. Yamasaki, F. Sakamoto, Y. Tani, Fungus-promoted transformation of lanthanides during the biooxidation of divalent manganese, Geochim. Cosmochim. Acta 174 (2016) 1–12.
[22] W.C. Song, X.X. Wang, Z.S. Chen, G.D. Sheng, T. Hayat, X.K. Wang, Y.B. Sun, Enhanced immobilization of U(VI) on *Mucor circinelloides* in presence of As(V): batch and XAFS investigation, Environ. Pollut. 237 (2018) 228–236.
[23] O.A. Vereshchagina, A.S. Memorskaya, V.M. Tereshina, Effect of trehalose on the viability of sporangiospores of the mucorous fungus *blakeslea trispora*, Microbiology 80 (2011) 775–783.
[24] S. China, B. Wang, J. Weis, L. Rizzo, J. Brito, G.G. Cirino, L. Kovarik, P. Artaxo, M.K. Gilles, A. Laskin, Rupturing of biological spores as a source of secondary particles in amazonia, Environ. Sci. Technol. 50 (2016) 12179–12186.
[25] N. Shlezinger, H. Irmer, S. Dhingra, S.R. Beattie, R.A. Cramer, G.H. Braus, A. Sharon, T.M. Hohl, Sterilizing immunity in the lung relies on targeting fungal apoptosis-like programmed cell death, Science 357 (2017) 1037–1041.
[26] K.U. Ulrich, A. Singh, E.J. Schofield, J.R. Bargar, H. Veeramani, J.O. Sharp, R. Bernier-Latmani, D.E. Giammar, Dissolution of biogenic and synthetic UO_2 under varied reducing conditions, Environ. Sci. Technol. 42 (2008) 5600–5606.
[27] B. Ravel, M. Newville, ATHENA, ARTEMIS, HEPHAESTUS: data analysis for X-ray absorption spectroscopy using IFEFFIT, J. Synchrotron Radiat. 12 (2005) 537–541.
[28] N.M. Esa, K.K.A. Kadir, Z. Amom, A. Azlan, Antioxidant activity of white rice, brown rice and germinated brown rice (in vivo and in vitro) and the effects on lipid peroxidation and liver enzymes in *hyperlipidaemic rabbits*, Food Chem. 141 (2013) 1306–1312.
[29] C.M. Rico, M.I. Morales, R. McCreary, H. Castillo-Michel, A.C. Barrios, J. Hong, A. Tafoy, W.Y. Lee, A. Varela-Ramirez, J.R. Peralta-Videa, J.L. Gardea-Torresdey, Cerium oxide nanoparticles modify the antioxidative stress enzyme activities and macromolecule composition in rice seedlings, Environ. Sci. Technol. 47 (2013) 14110–14118.
[30] J.Y. Wang, C.W. Cui, Characterization of the biosorption properties of dormant spores of *Aspergillus niger*: a potential breakthrough agent for removing Cu^{2+} from contaminated water, RSC Adv. 7 (2017) 14069–14077.
[31] A. Rosenhahn, J.A. Finlay, M.E. Pettit, A. Ward, W. Wirges, R. Gerhard, M.E. Callow, M. Grunze, J.A. Callow, Zeta potential of motile spores of the green alga Ulva linza and the influence of electrostatic interactions on spore settlement and adhesion strength, Biointerphases 4 (2009) 7–11.
[32] M. Donmez, M.D. Yilmaz, B. Kilbas, Fluorescent detection of dipicolinic acid as a biomarker of bacterial spores using lanthanide-chelated gold nanoparticles, J. Hazard. Mater. 324 (2017) 593–598.
[33] S. Srivastava, I.S. Thakur, Biosorption potency of *Aspergillus niger* for removal of chromium (VI), Curr. Microbial. 53 (2006) 232–237.
[34] M.T. El-Sayed, An investigation on tolerance and biosorption potential of *Aspergillus awamori* ZU JQ 965830.1 to Cd(II), Ann. Microbiol. 65 (2015) 69–83.
[35] P. Li, J. Wang, X. Wang, B. He, D. Pan, J. Liang, F.K. Wang, Q.H. Fan, Arsenazo-functionalized magnetic carbon composite for uranium (VI) removal from aqueous solution, J. Mol. Liq. 269 (2018) 441–449.
[36] J.P. Gustafsson, A windows version of MINTEQ. < http://www.lwr.kth.se/English/OurSOrware/vminteq/index.htm > , 2009.
[37] K. Tsekova, D. Todorova, S. Ganeva, Removal of heavy metals from industrial wastewater by free and immobilized cells of *Aspergillus niger*, Int. Biodeter. Biodegr. 64 (2010) 447–451.
[38] Q.H. Fan, L.M. Hao, C.L. Wang, Z. Zheng, C.L. Liu, W.S. Wu, The adsorption behavior of U (VI) on granite, Environ. Sci.: Processes Impacts 16 (3) (2014) 534–541.
[39] D.Q. Pan, Q.H. Fan, F.Y. Fan, Y.F. Tang, Y.Y. Zhang, W.S. Wu, Removal of uranium contaminant from aqueous solution by chitosan@attapulgite composite, Sep. Purif. Technol. 177 (2017) 86–93.
[40] S. Arora, J. Jain, J.M. Rajwade, K.M. Paknikar, Cellular responses induced by silver nanoparticles: in vitro studies, Toxicol. Lett. 179 (2008) 93–100.
[41] U. Krengel, S. Törnrothhorsefield, Coping with oxidative stress, Science 347 (2015) 7–10.
[42] H. Tian, S. Qu, Y. Wang, Z. Lu, M. Zhang, Y. Gan, P. Zhang, J. Tian, Calcium and oxidative stress mediate perillaldehyde-induced apoptosis in *Candida albicans*, Appl. Microbiol. Biotechnol. 101 (2017) 3335–3345.
[43] M. Montibus, L. Pinson-Gadais, F. Richard-Forget, C. Barreau, N. Ponts, Coupling of transcriptional response to oxidative stress and secondary metabolism regulation in filamentous fungi, Crit. Rev. Microbiol. 41 (2015) 295–308.
[44] Y. Yin, X. Yang, L. Hu, Z. Tan, L. Zhao, Z. Zhang, J. Liu, G. Jiang, Effect of salt stress on antioxidative enzymes and lipid peroxidation in leaves and roots of salt-tolerant and salt-sensitive maize genotypes, Environ. Sci. Technol. Lett. 3 (2016) 160–165.
[45] A.D. Azevedo Neto, J.T. Prisco, J. Enéas-Filho, C.E.B. Abreu, E. Gomes-Filho, Superoxide-mediated extracellular biosynthesis of silver nanoparticles by the fungus *Fusarium oxysporum*, Environ. Exp. Bot. 56 (2006) 87–94.
[46] E.J. O'Loughlin, S.D. Kelly, K.M. Kemner, XAFS investigation of the interactions of U(VI) with secondary mineralization products from the bioreduction of Fe(III) oxides, Environ. Sci. Technol. 44 (2010) 1656–1661.
[47] L.D. Troyer, Y. Tang, T. Borch, Simultaneous reduction of arsenic(V) and uranium (VI) by mackinawite: role of uranyl arsenate precipitate formation, Environ. Sci. Technol. 48 (2014) 14326–14334.
[48] Y.B. Sun, Z.Y. Wu, X.X. Wang, C.C. Ding, W.C. Cheng, S.H. Yu, X.K. Wang, Macroscopic and microscopic investigation of U(VI) and Eu(III) adsorption on carbonaceous nanofibers, Environ. Sci. Technol. 50 (2016) 4459–4467.
[49] H. Smith, S. Doyl, R. Murphy, Filamentous fungi as a source of natural antioxidants, Food Chem. 185 (2015) 389–397.
[50] C.D. Auwer, I. Llorens, P. Moisy, C. Vidaud, F. Goudard, C. Barbot, P.L. Solari, H. Funke, Actinide uptake by transferrin and ferritin metalloproteins, Radiochim. Acta 93 (2005) 699–703.
[51] S.V. Wegner, H. Boyaci, H. Chen, M.P. Jensen, C. He, Engineering A uranyl-specific binding protein from NikR, Angew. Chem. Int. Edit. 48 (2009) 2339–2341.
[52] H. Liu, Y. Zhu, B. Xu, P. Li, Y. Sun, T. Chen, Mechanical investigation of U(VI) on pyrrhotite by batch, EXAFS and modeling techniques, J. Hazard. Mater. 322 (2017) 488–498.
[53] K.E. Fletcher, M.I. Boyanov, S.H. Thomas, Q. Wu, K.M. Kemner, F.E. Löffler, U(VI) reduction to mononuclear U (IV) by *Desulfitobacterium* species, Environ. Sci. Technol. 44 (2010) 4705–4709.
[54] R. Bernier-Latmani, H. Veeramani, E.D. Vecchia, P. Junier, J.S. Lezama-Pacheco, E.I. Suvorova, J.O. Sharp, N.S. Wigginton, J.R. Bargar, Non-uraninite products of microbial U(VI) reduction, Environ. Sci. Technol. 44 (2010) 9456–9462.
[55] F. Gharib, A. Shamel, F. Lotfi, Ionic strength dependence of formation constants, complexation of glycine with dioxouranium(VI) ion, Rev. Inorg. Chem. 25 (2005) 361–372.
[56] A.D. Keramidas, M.P. Rikkou, C. Drouza, C.P. Raptopoulou, A. Terzis, I. Pashalidis, Synthesis and structural studies of the uranyl complexes with glycine and N-(2-mercaptopropionyl) glycine, Radiochim. Acta 90 (2002) 549–554.